COMPUTATIONALLY EFFICIENT TWO-OBJECTIVE OPTIMIZATION OF COMPACT MICROWAVE COUPLERS THROUGH CORRECTED DOMAIN PATCHING

Sławomir Kozieł[1, 2], Adrian Bekasiewicz[1, 2]

1) *Reykjavik University, Engineering Optimization & Modeling Center, School of Science and Engineering, 101 Reykjavik, Iceland* (*koziel@ru.is,* ✉ *bekasiewicz@ru.is,* + 354 599 6886)

2) *Gdańsk University of Technology, Faculty of Electronics, Telecommunications and Informatics, G. Narutowicza 11/12, 80-233 Gdańsk, Poland*

Abstract

Finding an acceptable compromise between various objectives is a necessity in the design of contemporary microwave components and circuits. A primary reason is that most objectives are at least partially conflicting. For compact microwave structures, the design trade-offs are normally related to the circuit size and its electrical performance. In order to obtain comprehensive information about the best possible trade-offs, multi-objective optimization is necessary that leads to identifying a Pareto set. Here, a framework for fast multi-objective design of compact micro-strip couplers is discussed. We use a sequential domain patching (SDP) algorithm for numerically efficient handling of the structure bandwidth and the footprint area. Low cost of the process is ensured by executing SDP at the low-fidelity model level. Due to its bi-objective implementation, SDP cannot control the power split error of the coupler, the value of which may become unacceptably high along the initial Pareto set. Here, we propose a procedure for correction of the *S*-parameters' characteristics of Pareto designs. The method exploits gradients of power split and bandwidth estimated using finite differentiation at the patch centres. The gradient data are used to correct the power split ratio while leaving the operational bandwidth of the structure at hand intact. The correction does not affect the computational cost of the design process because perturbations are pre-generated by SDP. The final Pareto set is obtained upon refining the corrected designs to the high-fidelity EM model level. The proposed technique is demonstrated using two compact microstrip rat-race couplers. Experimental validation is also provided.

Keywords: computer-aided design, compact circuits, microwave couplers, multi-objective optimization, domain patching, surrogate modelling, response correction.

1. Introduction

Circuit miniaturization, and, consequently, development of techniques for size reduction of structures and systems, has become an important topic in microwave and antenna design [1–6]. The main motivation is the practical necessity, specifically, increasing the number of space-limited applications such as in mobile communication and wearable devices [7, 8], as well as, recently, internet of things [9, 10]. One of the fundamental difficulties pertinent to compact mi-

crowave circuit design is that attempts to reduce the size of the structure normally lead to degradation of its electrical performance. In other words, these objectives are conflicting. Any practical design is a compromise between geometry- and electrical performance-related criteria [11, 12].

In terms of geometry modification, the most popular size reduction methods include bending and meandering of conventional transmission lines (TLs), as well as replacing them by compact slow-wave resonant cells that feature similar electrical characteristics as TLs (within a reduced frequency range) and shortened length [13, 14]. An important problem that arises here is that the aforementioned topological modifications increase electromagnetic (EM) cross-couplings within the structure. As a result, equivalent circuit models commonly used in the design process become unreliable. As a matter of fact, the only way of obtaining accurate evaluation of a compact circuit is its full-wave EM simulation. At the same time, accurate high-fidelity EM analysis is computationally expensive. Needless to say, a high evaluation cost is a serious bottleneck for simulation-driven design closure otherwise indispensable for tuning of the circuit parameters. Another practical problem is that size reduction by geometry modification increases the number of design variables that need to be adjusted: a typical compact cell is described by four to six parameters compared with only two needed for a TL. Both the aforementioned factors (high simulation cost and increased number of parameters) hinder the usage of conventional optimization techniques. As a workaround, the EM-driven design process of compact structures is commonly carried out by parameter sweeping. Such an interactive approach incorporates engineering experience and enables to find a reasonable (although not optimal) design solution. It should also be mentioned that an experience-driven design is virtually unable of explicit control of the circuit size. Typically, size reduction is achieved by appropriate selection of the circuit topology (e.g. [1–3, 13, 16]), whereas the design closure process itself only aims at achieving acceptable electrical performance.

Computationally-efficient optimization can be performed using surrogate-assisted techniques [17–19], by exploiting adjoints sensitivities [20, 21], or by a combination of both approaches (e.g. [22, 23]).

In practical design, it is useful to acquire comprehensive information about the best possible trade-offs between conflicting design criteria. In the case of compact circuits, these would be their structure size and electrical performance figures. Such information can be obtained through multi-objective optimization the result of which is typically in the form of a set of alternative designs representing a so-called Pareto front [24]. Among available methods, the most commonly used ones are undoubtedly population-based metaheuristics such as genetic algorithms [25, 26], particle swarm optimizers (PSO) [27, 28], or modified algorithms for constrained problems [38, 39]. Their popularity is mostly due to the capability of yielding the entire Pareto front representation in a single algorithm run. Nevertheless, due to their high cost (thousands and tens of thousands of objective function evaluations [30]) such methods are not practical for handling expensive EM simulation models. Modelling methods for constrained multi-objective optimization aimed at identification of a feasible region of search space have been introduced in [40–42]. However, curse of dimensionality limits usefulness of these techniques to problems with a small number of design variables. Efficient surrogate-assisted multi-objective design methods have been proposed in the context of antenna design [31, 32]. The key ideas employed in these methods include design space reduction and setting up a fast data-driven surrogate that can be directly optimized using metaheuristic algorithms so as to identify the initial Pareto set. Response correction methods are subsequently applied to fine tuning of a selected Pareto-optimal design [33].

The purpose of this work is to develop and demonstrate a technique for accelerated bi-objective design optimization of compact micro-strip couplers. Our approach exploits a sequential domain patching (SDP) technique [34, 43]. It creates a path connecting the two extreme

Pareto-optimal designs obtained by single-objective SBO processes (one oriented towards size reduction, the other aiming at bandwidth maximization). Unfortunately, in the case of coupler structures, it is also necessary to account for other circuit characteristics, specifically, to ensure equal power split. The approach discussed here is based on [44]. However, here, we focus on comprehensive description of the correction step for precise control of power split error of the initial Pareto-optimal designs generated by SDP. At the same time, a response refinement algorithm enables to control the coupler bandwidth so that it is not degraded while correcting the power split. Our approach is illustrated using two miniaturized rat-race couplers operating at 1 GHz. Experimental verification is also provided.

2. Two-Objective Optimization Using Sequential Domain Patching

In this section, in order to make the paper self-contained, a basic formulation of the sequential domain patching (SDP) algorithm is briefly recalled. A corrected SDP (CSDP) algorithm for bi-objective optimization (here, of micro-strip couplers) is presented in Section 3.

2.1. Multi-Objective Optimization Problem

We begin by formulating the multi-objective design optimization problem. Let $F_k(\mathbf{x})$, $k = 1$, ..., N_{obj}, be the kth objective. For $N_{obj} > 1$, the designs $\mathbf{x}$ and $\mathbf{y}$ can be compared using the Pareto dominance relation: $\mathbf{x} \prec \mathbf{y}$ ($\mathbf{x}$ dominates $\mathbf{y}$) if $F_k(\mathbf{x}) \leq F_k(\mathbf{y})$ for all k and $F_k(\mathbf{x}) < F_k(\mathbf{y})$ for at least one k [25]. The aim of the optimization process is to find a representation of a Pareto front X_P of the design space X, such that for any $\mathbf{x} \in X_P$, there is no $\mathbf{y} \in X$ for which $\mathbf{y} \prec \mathbf{x}$ [25]. Clearly, without loss of generality, maximization of $F_k(\mathbf{x})$ can be formulated as minimization of $-F_k(\mathbf{x})$.

The main focus of this work is the design of microwave couplers, which are a representative example of structures with multiple design criteria. We consider two (explicit) objectives: (i) the circuit area $F_1(\mathbf{x}) = A(\mathbf{x})$ and (ii) the coupler bandwidth $F_2(\mathbf{x}) = B(\mathbf{x})$. The bandwidth is defined as a range of frequencies for which both $|S_{11}|$ and $|S_{41}|$ are below -20 dB. Thus, an implicit design criterion is to design the circuit for a given operating frequency f_0. Furthermore, a power split error $d_s = |S_{21}| - |S_{31}|$ should be between -0.2 dB and $+0.2$ dB at f_0.

2.2. Sequential Domain Patching Algorithm

Our main optimization engine is the bi-objective sequential domain patching (SDP) algorithm. The initial stage of the SDP process is to identify the "extreme" Pareto designs $\mathbf{x}_k^*$, $k = 1$, ..., N_{obj}. These designs are obtained by solving single-objective optimization problems of the form [31]:

$$\mathbf{x}_k^* = \arg \min_{\mathbf{x}} F_k(\mathbf{R}_c(\mathbf{x})). \tag{1}$$

It should be noted that the extreme Pareto-optimal designs are being found at the level of a low-fidelity model $\mathbf{R}_c$ (which in our case is a coarse-discretization version of the high-fidelity EM model). This enables to reduce the cost of the algorithm.

The next step of the optimization process is to find a path connecting the designs $\mathbf{x}_k^*$, which is created by using the algorithm outlined below [34] (the design space dimensionality is denoted as n):

1. Set the patch size $\mathbf{p} = [p_1 \ldots p_n]^T$ (cf. Section 2.3);
2. Set the current points $\mathbf{x}_{c1} = \mathbf{x}_1^*$ and $\mathbf{x}_{c2} = \mathbf{x}_2^*$;

3. Evaluate n perturbations of size $\boldsymbol{p}$ around $\boldsymbol{x}^*_{c1}$ (towards $\boldsymbol{x}^*_{c2}$ only) and select the best one with respect to F_2;
4. Centre the patch at the point selected in Step 3; update $\boldsymbol{x}_{c1}$;
5. Evaluate n perturbations of size $\boldsymbol{p}$ around $\boldsymbol{x}^*_{c2}$ (towards $\boldsymbol{x}^*_{c1}$ only) and select the best one with respect to F_1.
6. Centre the patch at the point selected in Step 5; update $\boldsymbol{x}_{c2}$;
7. If the path between $\boldsymbol{x}^*_1$ and $\boldsymbol{x}^*_2$ is not complete, go to 3;

Figure 1 graphically illustrates the algorithm operation in the case of a three-dimensional design space. The non-dominated designs selected from the patch centres constitute the initial approximation of the Pareto front. It is interesting to note that the computational cost of the SDP algorithm depends only on the design space dimensionality n and on the total number of patches. More specifically, it can be bounded from above (excluding the cost of solving (1)) as $(M-1) \cdot (n-1)$, where $M = \sum_{j=1,...n} m_j$, and m_j is the number of intervals in the direction j. Another and perhaps even more important advantage of SDP over other bi-objective optimization techniques (including the recent surrogate-assisted methods [31–33]) is that there is no need for constructing of an auxiliary global response surface approximation model (i.e. a model valid over the entire design space considered) nor using population-based metaheuristics.
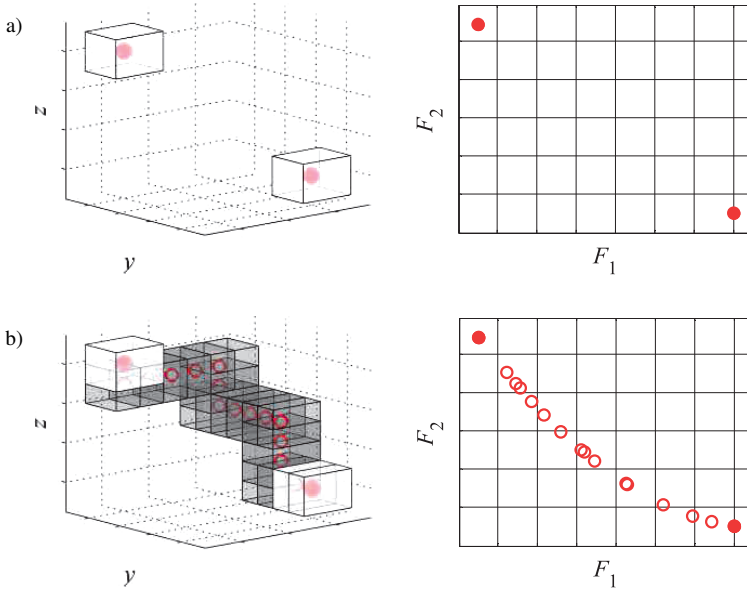

Fig. 1. A conceptual illustration of the SDP algorithm for the design problem with $n = 3$ variables: a) "extreme" Pareto optimal designs obtained through sequential single-objective optimizations (●); b) Pareto-optimal solutions obtained using the discussed procedure (○). The left panel figures represent the domain space; the right panel figures represent the feature space.

2.3. Patch Size Determination

The numbers of intervals m_j between $\boldsymbol{x}^*_1$ and $\boldsymbol{x}^*_2$ in each direction have to be integers. At the same time, the numbers m_j should be determined so that the changes of the model response (within a patch) are comparable for all dimensions. In this work, the vector of intervals M is obtained as follows (we use the notation $\boldsymbol{x}^*_1 = [x^*_{1.1} \dots x^*_{1.n}]^T$, similarly for $\boldsymbol{x}^*_2$):

1. Evaluate $\boldsymbol{R}_c$ at n points $\boldsymbol{x}_{1-2}^{(j)} = [x_{1.1}^* \ \ldots x_{1.j-1}^* x_{2.j}^* x_{1.j+1}^* \ \ldots x_{1.n}^*]^T$ and calculate $E_{1.j} = \|\boldsymbol{R}_c(\boldsymbol{x}_{1-2}^{(j)}) - \boldsymbol{R}_c(\boldsymbol{x}_1^*)\| / \|\boldsymbol{R}_c(\boldsymbol{x}_1^*)\|$;

2. Evaluate $\boldsymbol{R}_c$ at n points $\boldsymbol{x}_{2-1}^{(j)} = [x_{2.1}^* \ \ldots x_{2.j-1}^* x_{1.j}^* x_{2.j+1}^* \ \ldots x_{2.n}^*]^T$ and calculate $E_{2.j} = \|\boldsymbol{R}_c(\boldsymbol{x}_{2-1}^{(j)}) - \boldsymbol{R}_c(\boldsymbol{x}_2^*)\| / \|\boldsymbol{R}_c(\boldsymbol{x}_2^*)\|$;

3. Set $E_j = (E_{1.j} + E_{2.j})/2$;

4. Normalize $E_j = E_j / \max\{E_j : \ j = 1, \ldots, n\}$;

5. Set $m_j = \max\left\{2, \lceil m_{\max} \cdot E_j \rceil\right\}$.

In the above procedure, the relative changes of the system responses are represented by $E_{1.j}$, $j = 1, \ldots, n$, obtained by varying the jth component of $\boldsymbol{x}_1^*$ towards $\boldsymbol{x}_2^*$ (definition of $E_{2.j}$ is similar); E_j are their average values and represent large-scale sensitivities of the circuit. Using these, the number of intervals along the jth axis is set proportional to E_j. The minimum number of intervals is 2; the maximum number of intervals is m_{max} and it is the only control parameter that needs to be set by the user.

2.4. Pareto Set Refinement

The initial Pareto set is obtained at the level of a low-fidelity model $\boldsymbol{R}_c$. Thus, the last stage of the optimization process is to yield Pareto-optimal designs for the high-fidelity model $\boldsymbol{R}_f$. In order to do so, the following refinement process is executed for the designs $\boldsymbol{x}_c^{(k)}$, $k = 1, \ldots, K$, selected from the initial front (here, $\boldsymbol{x}_f^{(k)} = \boldsymbol{x}_c^{(k)}$ [34]:

$$\boldsymbol{x}_f^{(k)} \leftarrow \arg \min_{\boldsymbol{x}, F_2(\boldsymbol{x}) \leq F_2(\boldsymbol{x}_j^{(k)})} F_1\left(\boldsymbol{R}_s(x) + d\boldsymbol{R}^{(k)}\right), \tag{2}$$

where $d\boldsymbol{R}^{(k)} = \boldsymbol{R}_f(\boldsymbol{x}_f^{(k)}) - \boldsymbol{R}_s(\boldsymbol{x}_f^{(k)})$. This correction term ensures perfect agreement between the surrogate and the high-fidelity model at the beginning of the refinement iteration. The purpose of the refinement process is to improve the first objective as much as possible without compromising the second objective. In practice, up to two iterations of (2) – three evaluations of the R_f model – are sufficient. The surrogate $\boldsymbol{R}_s$ is a second-order polynomial approximation (without mixed terms) of $\boldsymbol{R}_c$, constructed using evaluations of $\boldsymbol{R}_c$ at $\boldsymbol{x}_c^{(k)}$ and $2n$ perturbations around it. Note that half of the necessary perturbations are already available as they were evaluated during the SDP algorithm run.

3. Corrected SDP for Two-Objective Optimization of Miniaturized Couplers

The SDP algorithm as formulated in Section 2 handles two primary objectives, the circuit area and its bandwidth. However, the power split error d_s may be degraded along the path found by SDP, even though it is acceptable at the extreme Pareto-optimal designs. This is because d_s is not explicitly controlled during the optimization process. The design refinement (2) that follows SDP may not be able to move d_s back to the acceptable level. As a way of handling this problem, a correction procedure is proposed here which is applied to all designs selected from the Pareto front, $\boldsymbol{x}_c^{(k)}$, $k = 1, \ldots, K$, but before executing the refinement procedure (2). The correction process has to be arranged in such a way that it does not lead to significant degradation of the coupler bandwidth.

We will use $d_s(\mathbf{x}_c^{(k)})$ to denote the power split error at the design $\mathbf{x}_c^{(k)}$. Let $\nabla_s(\mathbf{x}_c^{(k)})$ be the estimated gradient of d_s at $\mathbf{x}_c^{(k)}$ with respect to the geometry parameters of the coupler. The gradient is obtained using finite differentiation based on the design perturbations within the patch corresponding to $\mathbf{x}_c^{(k)}$. It should be emphasized that the gradient estimation does not incur any computational overhead because the perturbations are already available: they were evaluated during the execution of the SDP algorithm. Similarly, we denote by $B(\mathbf{x}_c^{(k)})$ the coupler bandwidth at the design $\mathbf{x}_c^{(k)}$, and by $\nabla_B(\mathbf{x}_c^{(k)})$ the gradient of B at $\mathbf{x}_c^{(k)}$ estimated in the same way as for the power split error gradient.

The corrected design $\mathbf{x}_{c.corr}^{(k)}$ that brings the power split error to a required value d_t, and, at the same time, does not affect the coupler bandwidth, can be found by solving the following system of equations:

$$
\begin{bmatrix} d_s(\mathbf{x}_c^{(k)}) + \nabla_s^T(\mathbf{x}_c^{(k)}) \cdot (\mathbf{x}_{c.corr}^{(k)} - \mathbf{x}_c^{(k)}) \\ B(\mathbf{x}_c^{(k)}) + \nabla_B^T(\mathbf{x}_c^{(k)}) \cdot (\mathbf{x}_{c.corr}^{(k)} - \mathbf{x}_c^{(k)}) \end{bmatrix} = \begin{bmatrix} d_t \\ B(\mathbf{x}_c^{(k)}) \end{bmatrix}. \tag{3}
$$

Assuming that dimensionality of the design space is larger than two (which is the case for any practical compact coupler structure), the equation (3) is an underdetermined system with infinitely many solutions. We look for a solution that satisfies

$$
\mathbf{x}_{c.corr}^{(k)} = \min \left\{ \|\mathbf{y}\| : \begin{bmatrix} \nabla_s^T(\mathbf{x}_c^{(k)}) \cdot (\mathbf{y} - \mathbf{x}_c^{(k)}) \\ \nabla_B^T(\mathbf{x}_c^{(k)}) \cdot (\mathbf{y} - \mathbf{x}_c^{(k)}) \end{bmatrix} = \begin{bmatrix} -d_s(\mathbf{x}_c^{(k)}) + d_t \\ 0 \end{bmatrix} \right\}, \tag{4}
$$

i.e. reduces the power split error and does not change the coupler bandwidth while introducing the minimum (in the least-square sense) modification to the current design. This solution can be found as

$$
\mathbf{x}_{c.corr}^{(k)} = \mathbf{x}_c^{(k)} - \mathbf{A}^T (\mathbf{A}\mathbf{A}^T) \cdot \begin{bmatrix} d_s(\mathbf{x}_c^{(k)}) - d_t \\ 0 \end{bmatrix} \tag{5}
$$

where

$$
\mathbf{A} = \begin{bmatrix} \nabla_s^T(\mathbf{x}_c^{(k)}) \\ \nabla_B^T(\mathbf{x}_c^{(k)}) \end{bmatrix}. \tag{6}
$$

Note that, in principle, the value of d_t could be set to zero to achieve a perfect power split. In practice, other values, e.g. $d_t = 0.1$ dB, can be used to reduce the amount of correction (recall that the maximum absolute error according to design specifications is 0.2 dB). The reason is that requesting $d_t = 0$ might result in a larger correction (in terms of the norm-wise distance between the corrected and uncorrected design) and, consequently, potential degradation of the primary objectives. At the same time, the amount of correction is additionally controlled by the requirement of maintaining the circuit bandwidth (the second equation in (3)).

There are two practical issues that have to be addressed in practical implementation of the method. The first is that the coupler bandwidth is determined by four frequencies corresponding to -20 dB level of $|S_{11}|$ and $|S_{41}|$ response. In any particular situation, the bandwidth may depend either on $|S_{11}|$ or on $|S_{41}|$, yet when only looking at $B(\mathbf{x}_c^{(k)})$ it is impossible to tell which one is

limiting factor. For the same reason, $B(\mathbf{x})$ is, in general, not differentiable with respect to $\mathbf{x}$. Therefore, in practical realization of the correction, it is better to replace (3) by

$$\begin{bmatrix} d_s(\mathbf{x}_c^{(k)}) + \nabla_s^T(\mathbf{x}_c^{(k)}) \cdot (\mathbf{x}_{c.corr}^{(k)} - \mathbf{x}_c^{(k)}) \\ B(\mathbf{x}_c^{(k)}) + \nabla_{F_B}^T(\mathbf{x}_c^{(k)}) \cdot (\mathbf{x}_{c.corr}^{(k)} - \mathbf{x}_c^{(k)}) \end{bmatrix} = \begin{bmatrix} d_t \\ F_B \mathbf{x}_c^{(k)} \end{bmatrix} \tag{7}$$

where $F_B(\mathbf{x}_c^{(k)}) = [f_{B1}(\mathbf{x}_c^{(k)})\ f_{B2}(\mathbf{x}_c^{(k)})\ f_{B3}(\mathbf{x}_c^{(k)})\ f_{B4}(\mathbf{x}_c^{(k)})]^T$, with $f_{Bk}(\mathbf{x}_c^{(k)})$, $k = 1, \ldots, 4$, being the four aforementioned frequencies. Keeping them fixed in the correction process ensures maintaining of the circuit bandwidth.

Replacing (3) by (7) results in reformulating the correction problem as

$$\mathbf{x}_{c.corr}^{(k)} = \min \left\{ \|\mathbf{y}\| : \begin{bmatrix} \nabla_s^T(\mathbf{x}_c^{(k)}) \cdot (\mathbf{y} - \mathbf{x}_c^{(k)}) \\ \nabla_{F_B}^T(\mathbf{x}_c^{(k)}) \cdot (\mathbf{y} - \mathbf{x}_c^{(k)}) \end{bmatrix} = \begin{bmatrix} -d_s(\mathbf{x}_c^{(k)}) + d_t \\ 0 \\ 0 \\ 0 \\ 0 \end{bmatrix} \right\}. \tag{8}$$

The analytical solution is

$$\mathbf{x}_{c.corr}^{(k)} = \mathbf{x}_c^{(k)} - A_F^T(A_F A_F^T) \cdot \begin{bmatrix} d_s(\mathbf{x}_c^{(k)}) - d_t \\ 0 \\ 0 \\ 0 \\ 0 \end{bmatrix}, \tag{9}$$

where

$$A_F = \begin{bmatrix} \nabla_s^T(\mathbf{x}_c^{(k)}) \\ \nabla_{F_B}^T(\mathbf{x}_c^{(k)}) \end{bmatrix}. \tag{10}$$

The second issue is that analytical solution to (8) given by (10) does not ensure that the corrected solution is located within the patch, the centre of which is the initial design (to be refined) $\mathbf{x}_c^{(k)}$. This can be ensured by solving (8) as a constrained nonlinear optimization problem with the constraint $\mathbf{l}_y \leq \mathbf{y} \leq \mathbf{u}_y$, where $\mathbf{l}_y$ and $\mathbf{u}_y$ are the lower and upper bounds for $\mathbf{y}$ defined as $\mathbf{l}_y = \mathbf{x}_c^{(k)} - \mathbf{p}$, and $\mathbf{u}_y = \mathbf{x}_c^{(k)} + \mathbf{p}$ ($\mathbf{p}$ is the patch size).

It should be mentioned that, in principle, a similar methodology as presented in this section could be applied to correct other types of figures of merit (not only the power split error). For example, in the case of couplers, this could be the operating frequency of a phase response. Clearly, the "amount" of correction is limited by the usage of first-order Taylor models, which is a trade-off between the correction reliability and the computational cost of it.

4. Case Study I: Folded Rat-Race Coupler

The purpose of this section is to demonstrate the corrected SDP algorithm. We consider bi-objective optimization of a rat-race micro-strip coupler miniaturized by folding its transmission line sections. We also examine the influence of a selected correction type on the algorithm performance, specifically, the quality of the final coupler designs obtained in the process. The selected high-fidelity Pareto designs are validated experimentally.

145

4.1. Coupler Structure

Consider a miniaturized rat-race coupler (RRC) circuit shown in Fig. 2 [12]. Small dimensions of the structure with respect to a conventional coupler [35] have been achieved by folding its quarter-wavelength sections. The RRC is implemented on a 0.762 mm thick Taconic RF-35 substrate ($\varepsilon_r = 3.5$, $\tan \delta = 0.018$). An operating frequency is 1 GHz. A vector of design variables is $\boldsymbol{x} = [l_1 \; l_2 \; l_3 \; d \; w]^T$. Dimensions $w_0 = 1.7$, $l_0 = 15$ remain fixed (all in mm). A high-fidelity EM model of the structure $\boldsymbol{R}_f$ is prepared in CST Microwave Studio [36]. It consists of about 220,000 mesh cells and its average simulation time on a dual Xeon E5540 machine is 15 minutes. A low-fidelity model $\boldsymbol{R}_c$ is also implemented in CST Studio. It consists of $\sim 26,000$ cells (simulation time: 84 seconds). The structure size is given as $A(\boldsymbol{x}) = 15w + 12d + l_1 + l_2 + l_3 + 2w_0$. The search space is defined by the following lower and upper bounds: $\boldsymbol{l} = [1 \; 5 \; 10 \; 0.2 \; 0.2]^T$ and $\boldsymbol{u} = [8 \; 15 \; 30 \; 1.2 \; 1.2]^T$.

4.2. Results

In the first step of the design process, the sequential single-objective optimizations (cf. Section 2.2) have been performed to find the extreme Pareto-optimal designs: $\boldsymbol{x}_1^* = [4.21 \; 11.65 \; 24.66 \; 0.27 \; 0.90]^T$ (the smallest footprint) and $\boldsymbol{x}_2^* = [3.86 \; 12.14 \; 20.14 \; 1.05 \; 0.86]^T$ (the broadest bandwidth). Then, the procedure of Section 2.3 has been used to obtain a vector of intervals $M = [2213153]$ and the patching algorithm has been executed. The initial Pareto set identified using SDP is shown in Fig. 3.
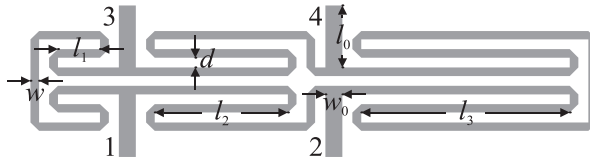

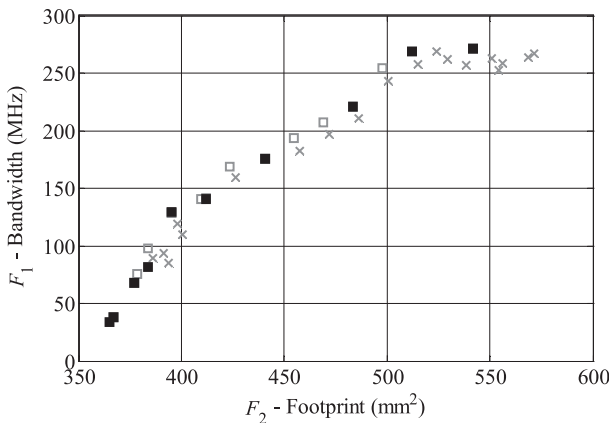Fig. 2. Geometry of the compact folded rat-race coupler [12].

Fig. 3. A low-fidelity Pareto set obtained using the SDP algorithm. Crosses and grey squares represent the dominated and non-dominated designs, respectively, whereas the designs selected for correction are marked with black squares.

It should be reiterated that the SDP algorithm can handle only two objectives at a time and thus there is no direct control in the optimization process over the power split between the coupler ports. At the same time, the power split error is supposed to be maintained within an acceptable bound (e.g. ± 0.2 dB). In order to handle this issue, the method of Section 3 is used for correction of the obtained Pareto designs. It should be emphasized that the correction step does not require any additional model simulations because all the data required for solving (8) were obtained by SDP. In this work, we have considered four variants of gradient-based correction (GC). The specific setups are as follows: (i) coupling threshold $d_t = 0$ dB, (ii) coupling threshold $d_t = 0$ dB and fixed bandwidth B; (iii) $d_t = 0.1$ dB; and (iv) $d_t = 0.1$ dB and fixed B. Note that imposing constraints on bandwidth (as in (ii) and (iv)) is expected to lead to some degradation of the power split error control.

Table 1 compares the results obtained for each correction variant with the responses of non-corrected (NC) coupler designs. The results indicate that each correction type has a different effect on the coupler responses. Although all the methods limit the 3 dB coupling error with respect to the reference designs, using the correction (i) and (iii) also results in narrowing the structure bandwidth with respect to all reference designs. On the other hand, this effect can be reduced when correction is performed using the method (ii) or (iv). At the same time, the approach (iv) produces designs that violate the imposed design specifications. Thus, in this work, the RRC correction is performed using the variant (ii). The influence of the gradient-based correction on the coupler responses on selected low-fidelity Pareto optimal designs is shown in Fig. 4.

Table 1. A folded RRC: Comparison of the Coupler Response Correction Methods.

	Correction type									
	NC		GC (i)		GC (ii) – selected		GC (iii)		GC (iv)	
	B	d_s	B	d_s	B	d_s	B	d_s	B	d_s
$x_c^{(1)}$	33.8	0.13	16.2	−0.01	34.4	−0.03	29.4	0.10	34.9	0.10
$x_c^{(2)}$	37.9	0.04	32.3	0.01	39.4	−0.01	32.3	0.01	39.4	−0.01
$x_c^{(3)}$	68.0	0.29	49.4	0.03	54.9	0.04	55.5	0.13	62.6	0.14
$x_c^{(4)}$	81.7	0.40	66.1	0.09	66.1	0.09	66.1	0.09	70.0	0.10
$x_c^{(5)}$	129.2	0.18	123.0	0.02	120.7	0.03	123.0	0.12	126.4	0.12
$x_c^{(6)}$	140.8	0.24	135.2	0.12	135.2	0.12	135.2	0.12	139.1	0.13
$x_c^{(7)}$	175.8	0.22	177.4	0.13	177.4	0.13	177.4	0.13	177.4	0.13
$x_c^{(8)}$	221.2	0.15	224.3	0.08	224.3	0.08	221.5	0.09	222.2	0.10
$x_c^{(9)}$	269.3	0.26	270.0	0.20	270.0	0.20	270.0	0.21	270.0	0.21
$x_c^{(10)}$	271.2	0.24	271.5	0.20	275.1	0.20	271.5	0.22	275.6	0.22

In the next step, the corrected low-fidelity designs have been refined to the high-fidelity model level using the method of Section 2.4. The dimensions of the high-fidelity Pareto designs are given in Table 2. The results indicate that miniaturization of the coupler designs with respect to a conventional rectangular RRC [35] vary from 87.8% to 92.2% along the Pareto front. The coupler with the smallest size of 354 mm^2 features a bandwidth of 68.3 MHz, whereas a bandwidth of the largest coupler design (553 mm^2) is 275 MHz. It should be noted that the power split error of the high-fidelity designs is within a -0.18 dB to 0.2 dB range, which is low – having in mind that the refinement process was performed without constraints imposed on d_s.
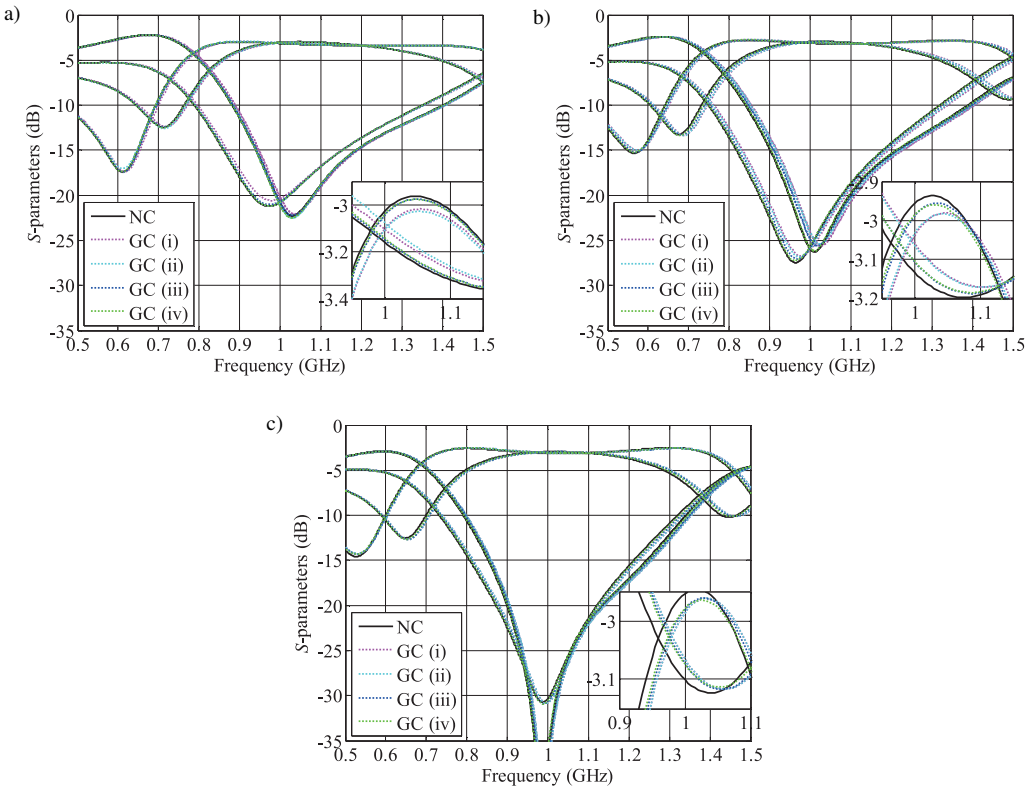
Fig. 4. A folded RRC: comparison of coupler responses for various correction methods (see Table 1) at the design: a) $x_c^{(1)}$; b) $x_c^{(5)}$; and c) $x_c^{(8)}$.

Table 2. High-Fidelity Designs of the Optimized Folded RRC.

		Coupler designs									
		$x_f^{(1)}$	$x_f^{(2)}$	$x_f^{(3)}$	$x_f^{(4)}$	$x_f^{(5)}$	$x_f^{(6)}$	$x_f^{(7)}$	$x_f^{(8)}$	$x_f^{(9)}$	$x_f^{(10)}$
Parameters	l_1	3.62	3.88	3.95	3.95	3.45	3.45	3.95	3.95	3.45	3.95
	l_2	12.8	12.1	12.0	12.0	13.0	13.0	12.0	12.0	12.5	12.0
	l_3	24.1	23.1	23.2	23.1	21.9	20.9	21.4	20.7	20.2	20.7
	d	0.29	0.39	0.40	0.45	0.61	0.76	0.71	0.82	1.00	0.97
	w	0.86	0.86	0.87	0.87	0.83	0.83	0.88	0.87	0.85	0.87
Size reduction* (%)		92.2	91.6	91.5	91.2	90.5	89.6	89.5	89.0	88.0	87.8

* With respect to conventional rectangular RRC (size: $47.5 \times 95.5 \approx 4536$ mm^2).

For the sake of comparison, the method of Section 2.4 was also used for refinement of the non-corrected low-fidelity Pareto designs. The results of Table 3 indicate that their power split errors vary from -0.04 dB to 0.39 dB which significantly violates the specification ($d_s \leq 0.2$ dB). In other words, for the considered design case, the gradient-based correction noticeably improves 3 dB coupling of the Pareto designs. The frequency characteristics of selected gradient-corrected and non-corrected high-fidelity model designs are compared in Fig. 5.

Table 3. RRC Optimization: High-Fidelity Model Responses.

	Corrected Pareto designs			Non-corrected Pareto designs		
	F_1	F_2	d_s	F_1	F_2	d_s
$\boldsymbol{x}_f^{(1)}$	68.3	354	−0.18	67.0	365	0.39
$\boldsymbol{x}_f^{(2)}$	132.0	380	0.13	92.9	374	−0.04
$\boldsymbol{x}_f^{(3)}$	135.3	384	0.19	99.4	384	0.38
$\boldsymbol{x}_f^{(4)}$	147.9	400	0.20	143.0	395	0.29
$\boldsymbol{x}_f^{(5)}$	185.8	430	−0.07	189.3	441	0.31
$\boldsymbol{x}_f^{(6)}$	236.9	473	−0.04	233.1	481	0.06
$\boldsymbol{x}_f^{(7)}$	241.2	476	0.20	238.6	483	0.27
$\boldsymbol{x}_f^{(8)}$	268.7	499	0.12	258.3	508	0.18
$\boldsymbol{x}_f^{(9)}$	269.6	546	0.12	274.3	552	0.15
$\boldsymbol{x}_f^{(10)}$	275.0	553	0.19	270.5	542	0.23
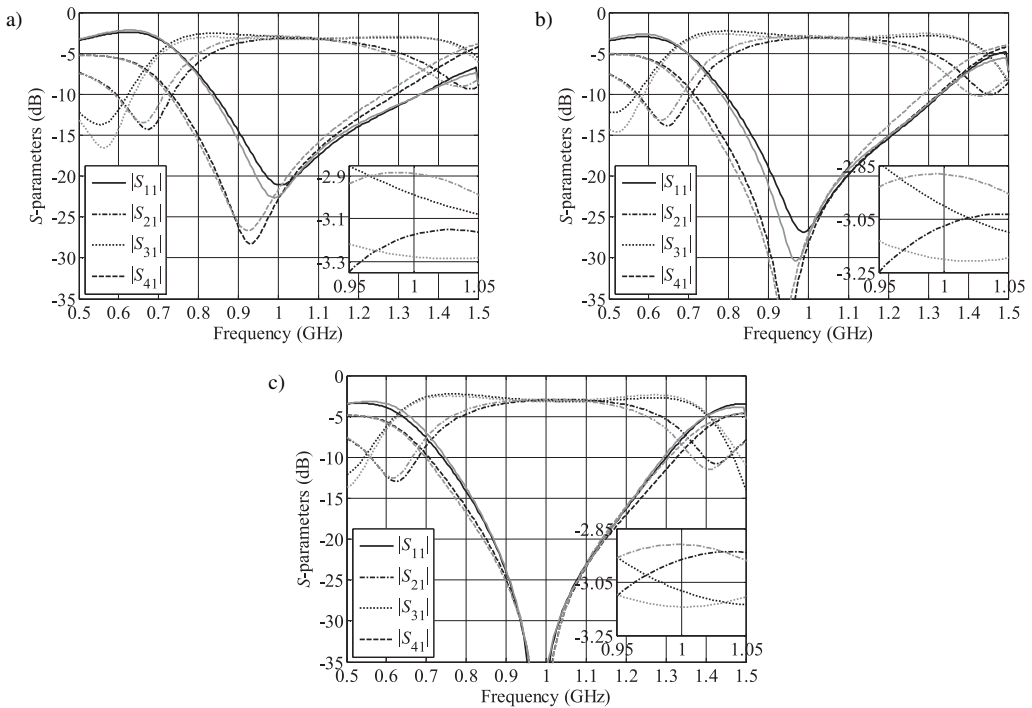
Fig. 5. A folded RRC: high-fidelity responses of the gradient-corrected (black lines) and non-corrected (grey lines) designs after the refinement process: a) $\boldsymbol{x}_f^{(1)}$, b) $\boldsymbol{x}_f^{(5)}$, and c) $\boldsymbol{x}_f^{(9)}$.

The cost of bi-objective optimization corresponds to ~68 simulations of the high-fidelity coupler model $\boldsymbol{R}_f$ (~17 hours of CPU-time), including 195 evaluations of the low-fidelity model $\boldsymbol{R}_c$ required to obtain the extreme Pareto-optimal designs, 10 $\boldsymbol{R}_c$ evaluations for determining the patch sizes for the SDP algorithm, 96 $\boldsymbol{R}_c$ simulations for determining the initial Pareto set using the SDP method, 10 $\boldsymbol{R}_c$ simulations for verification of the corrected low-fidelity designs, as well as 110 $\boldsymbol{R}_c$ and 30 $\boldsymbol{R}_f$ simulations to refine selected designs. Benchmarking of the pro-

posed approach is not provided because comprehensive tests already reported in the literature (e.g. [34, 43]) indicate superiority of SDP over other state-of-the-art algorithms in terms of numerical cost (even for problems with over ten design variables), whereas the correction stage does not incur any extra computational overhead, as already discussed. Also, the cost of our optimization-correction-refinement method is low compared to approaches dedicated for constrained optimization (population-based algorithms [38, 39] and methods for modelling feasible regions of the search space [40–42]), which require hundreds to thousands of model simulations for solving two-dimensional design problems.

4.3. Experimental Validation

The high-fidelity designs $x_f^{(1)}$, $x_f^{(5)}$, and $x_f^{(9)}$ have been fabricated and measured. Photographs of the manufactured coupler prototypes are shown in Fig. 6, whereas the simulated and measured characteristics of the structure are compared in Fig. 7. The results are in good agreement. The simulated and measured bandwidths are 269 MHz and 270 MHz for $x_f^{(1)}$, 186 MHz and 200 MHz for $x_f^{(5)}$, as well as 68 MHz and 60 MHz for $x_f^{(9)}$. At the same time, the power split errors are 0.19 dB and 0.20 dB for $x_f^{(1)}$, 0.1 dB and 0.18 dB for $x_f^{(5)}$, as well as 0.12 and 0.05 for $x_f^{(9)}$. It should be noted that increased losses for the measured designs are introduced by the SMA connectors which were not included in the computational EM model of the coupler.
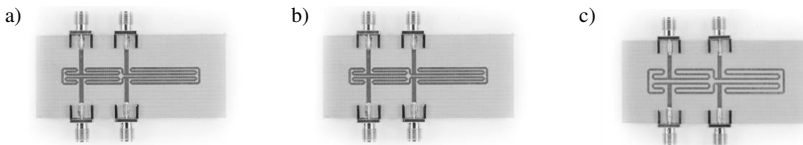

Fig. 6. Photographs of the manufactured designs of folded rat-race coupler: a) $x_f^{(1)}$, b) $x_f^{(5)}$, and c) $x_f^{(9)}$.
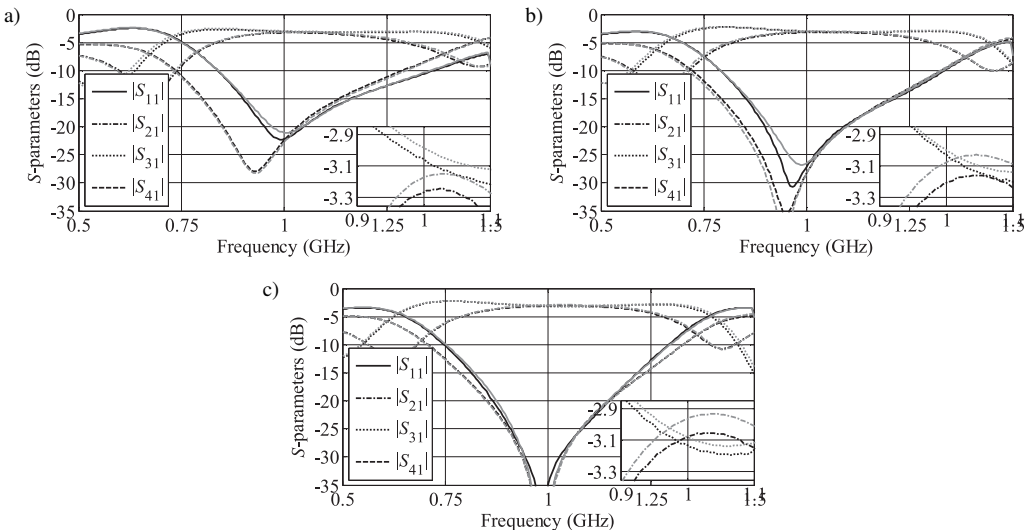

Fig. 7. A folded RRC: comparison of the simulated (grey lines) and measured (black lines) reflection characteristics. Designs: a) $x_f^{(1)}$, b) $x_f^{(5)}$, and c) $x_f^{(9)}$.

5. Case Study II: Miniaturized Rat–Race Coupler

Our second design case is a miniaturized rat-race coupler composed of compact microstrip resonant cells (CMRC). Two-objective optimization of the structure is performed using a gradient-corrected SDP algorithm. The numerical results are validated by measurements of the fabricated coupler prototypes.

5.1. Coupler Structure

Consider an RRC coupler shown in Fig. 8 [37]. The structure is miniaturized using six CMRC sections with shunt stubs. The substrate parameters are the same as for the coupler of Section 4. The centre frequency is set to 1 GHz. The design variables are: $x = [w\ d_1\ d_2\ l_2\ l_{3r}\ l_{4r}\ l_{5r}]^T$. The relative parameters are: $l_1 = 2d_1 + d_2 + 2.5w$, $l_3 = 0.1l_{3r}l_2$, $l_4 = 0.1l_{4r}l_3$, and $l_5 = 0.1l_{5r}l_2$, whereas the dimension $w_0 = 1.7$ remains fixed to ensure 50 ohm input impedance (all dimensions are in mm). Both, the high- ($\sim 350{,}000$ mesh cells; 23 min simulation) and low-fidelity ($\sim 128{,}000$ mesh cells; 230 s simulation) models of the structure are implemented in CST Microwave Studio [36]. The coupler area is defined as $A(x) = 35w + 24d_1 + 8d_2 + l_2$. The search space is defined by the following bounds: $l = [0.2\ 0.2\ 0.2\ 5\ 0.5\ 0.5\ 0.5]^T$ and $u = [1.2\ 3.2\ 3.2\ 15\ 10\ 10\ 10]^T$.
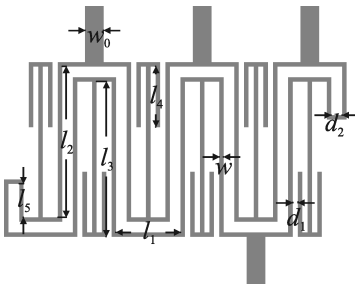

Fig. 8. Geometry of a compact CMRC-based rat-race coupler [37].

5.2. Results

The extreme Pareto-optimal designs with respect to size, $x_1^* = [0.21\ 0.5\ 1.02\ 13.32\ 10\ 9\ 2.61]^T$, and bandwidth, $x_2^* = [0.55\ 0.98\ 2.9\ 10.47\ 9.99\ 1.74\ 0.53]^T$, have been obtained using the sequential optimization algorithm of Section 2.2. Subsequently, the vector of intervals $M = [10\ 15\ 8\ 13\ 3\ 12\ 10]$ has been obtained and the SDP algorithm has been executed. The initial (low-fidelity) Pareto-optimal set is shown in Fig. 9. The ranges of the initial Pareto front along objectives F_1 and F_2 are 211 MHz and 525 mm^2, respectively.

In the next step, the responses of selected Pareto-optimal designs have been corrected using the method of Section 3 (correction setup: coupling threshold $d_t = 0$ dB and fixed bandwidth B). Table 4 provides comparison of the coupler responses for the gradient-corrected and non-corrected designs. The results indicate that the corrected designs maintain the requirement with respect to the acceptable power split error ($d_t \leq 0.2$ dB), which is not the case for a few of non-corrected designs. An average improvement of d_t for GC with respect to NC is 0.09 dB. At the same time, the bandwidth of the corrected designs is preserved within a 40-MHz margin with respect to the non-corrected ones. The frequency responses of selected GC and NC Pareto designs are compared in Fig. 10.

Finally, the selected Pareto designs have been refined using the method of Section 2.4. Detailed dimensions and performance parameters of the obtained high-fidelity Pareto set are gath-
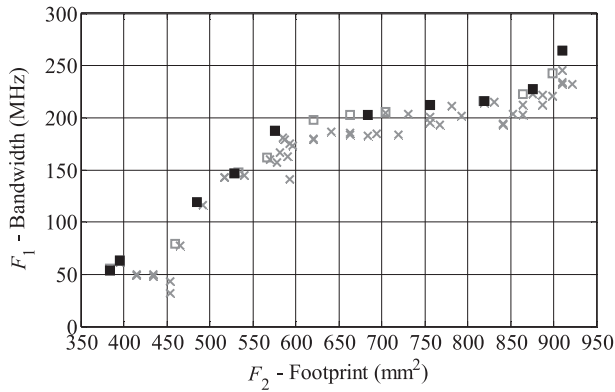
Fig. 9. A low-fidelity Pareto set obtained using the SDP algorithm:
non-dominated ($\square$), dominated ($\times$), and selected ($\blacksquare$) designs.

Table 4. A CMRC-Based RRC: Performance Comparison of Corrected (GC) and Non-Corrected (NC) Pareto Designs.

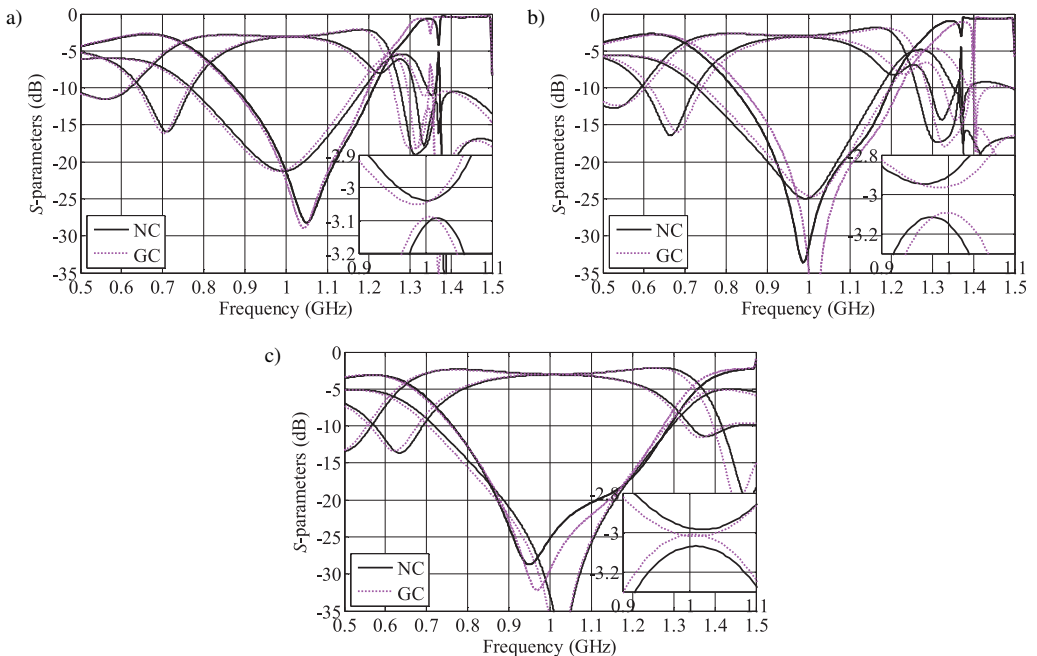|		Selected Pareto optimal designs									
		$x_c^{(1)}$	$x_c^{(2)}$	$x_c^{(3)}$	$x_c^{(4)}$	$x_c^{(5)}$	$x_c^{(6)}$	$x_c^{(7)}$	$x_c^{(8)}$	$x_c^{(9)}$	$x_c^{(10)}$
NC	B	264.1	227.3	216.3	212.2	202.4	187.1	146.7	118.9	63.5	53.3
GC		266.5	265.2	218.9	238.7	234.7	185.9	140.0	123.3	68.3	47.9
NC	d_s	−0.1	−0.09	−0.06	−0.1	−0.07	−0.13	−0.24	−0.21	−0.06	−0.07
GC		−0.01	0.01	−0.04	−0.08	−0.07	−0.12	−0.13	−0.19	−0.06	−0.04

Fig. 10. The frequency responses of a CMRC-based coupler for the corrected and non-corrected Pareto designs:
a) $x_c^{(2)}$; b) $x_c^{(7)}$; and c) $x_c^{(10)}$.

ered in Table 5. It should be noted that the variability of the coupler performance figures along the Pareto front are 234 MHz and 530 mm^2, with respect to F_1 and F_2, respectively. Moreover, the power split error d_s for the obtained designs varies from -0.08 dB to -0.16 dB. Also, miniaturization of the obtained Pareto designs with respect to a conventional RRC is 91.5% for the smallest structure (size: 387 mm^2, bandwidth: 38 MHz) and 80.3% for the design with the broadest bandwidth (size: 917 mm^2, bandwidth: 272 MHz). The frequency characteristics of selected high-fidelity Pareto designs are shown in Fig. 11.

Table 5. A CMRC-Based RRC: Optimized Designs.

		Coupler designs									
		$x_f^{(1)}$	$x_f^{(2)}$	$x_f^{(3)}$	$x_f^{(4)}$	$x_f^{(5)}$	$x_f^{(6)}$	$x_f^{(7)}$	$x_f^{(8)}$	$x_f^{(9)}$	$x_f^{(10)}$
F_1 (MHz)		38.1	62.9	126.2	141.1	155.1	180.1	198.5	232.9	247.9	272.2
F_2 (mm^2)		387	397	465	508	563	585	736	848	896	917
d_s (dB)		-0.08	-0.16	-0.12	-0.14	-0.13	-0.11	-0.13	-0.08	-0.08	-0.08
Parameters	w	0.20	0.20	0.30	0.29	0.29	0.33	0.50	0.50	0.53	0.53
	d_1	0.52	0.54	0.52	0.58	0.68	0.71	0.70	0.75	0.87	0.96
	d_2	1.01	1.04	1.32	1.48	1.91	1.84	2.31	3.14	3.02	3.02
	l_2	13.43	13.31	12.65	12.77	11.65	11.68	11.24	10.55	10.58	10.36
	l_{3r}	9.99	9.99	9.99	9.99	9.99	9.99	9.99	9.99	9.99	9.99
	l_{4r}	8.99	8.99	7.97	7.49	6.71	6.88	3.49	2.84	1.78	1.69
	l_{5r}	2.51	2.61	1.55	1.67	1.50	1.67	1.67	1.57	1.38	0.72
Reduction of size* (%)		91.5	91.5	91.2	89.8	88.8	87.6	87.1	83.8	81.3	80.3

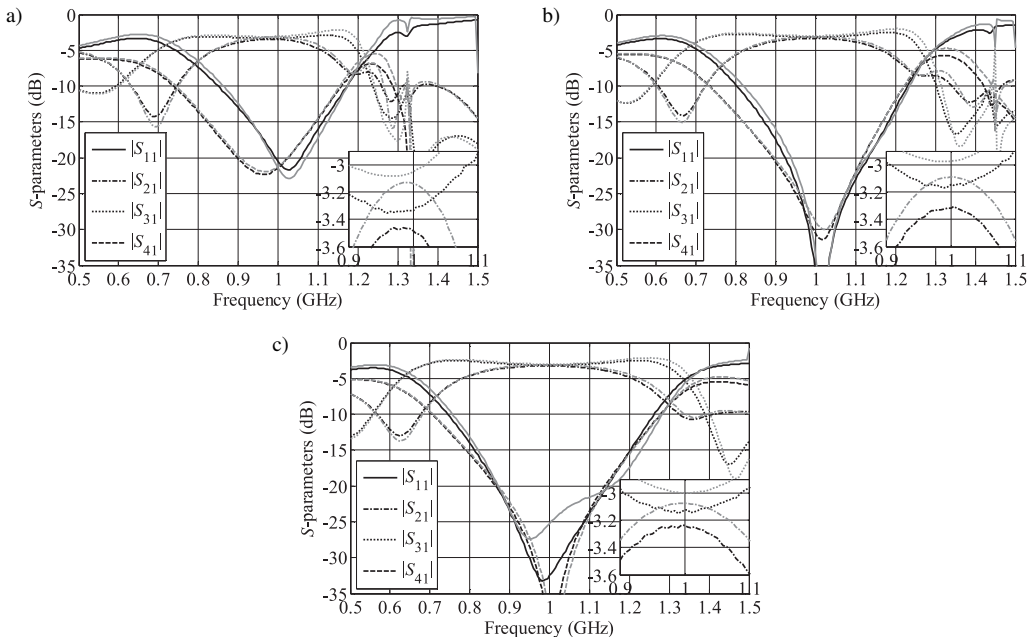* With respect to conventional rectangular RRC (size: $47.5 \times 95.5 \approx 4536$ mm^2).

Fig. 11. The simulated (grey lines) and measured (black lines) reflection characteristics of a CMRC-based RRC:
a) $x_f^{(1)}$, b) $x_f^{(6)}$, and c) $x_f^{(10)}$.

5.3. Experimental Validation

The designs $x_f^{(1)}$, $x_f^{(6)}$, and $x_f^{(10)}$ have been manufactured and measured. Photographs of the fabricated structures are shown in Fig. 12, whereas comparisons of their simulated and measured *S*-parameters' characteristics are given in Fig. 11. The results are in good agreement. The simulated and measured power split errors are -0.08 dB and -0.15 dB for $x_f^{(1)}$, -0.11 dB and -0.17 dB for $x_f^{(6)}$, as well as -0.08 and -0.11 for $x_f^{(10)}$. The simulated and measured bandwidths are 272 MHz and 270 MHz for $x_f^{(1)}$, 180 MHz and 190 MHz for $x_f^{(6)}$, as well as 38 MHz and 30 MHz for $x_f^{(10)}$. Similarly to the previous design case, the increased losses for the measurements are due to the SMA connectors (not included in the EM model, thus not accounted for in the design process). The discrepancies between simulation and measurement responses are also a result of fabrication tolerances.
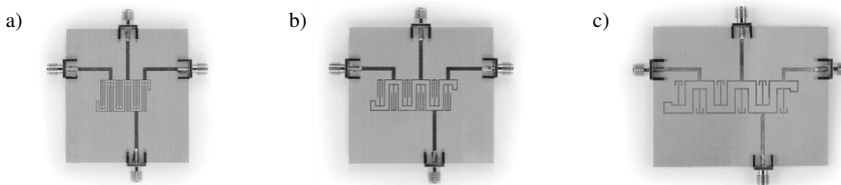

Fig. 12. Photographs of the manufactured CMRC-based coupler designs: a) $x_f^{(1)}$, b) $bmrx_f^{(5)}$, and (c) $x_f^{(10)}$.

6. Conclusion

In this paper, a reliable and deterministic procedure for accelerated bi-objective design optimization of miniaturized microwave couplers has been presented. The main optimization engine is a sequential domain patching algorithm (SDP). In order to achieve better control over the secondary objectives, specifically, the power split error and the coupler bandwidth, a procedure for correcting responses of the initial Pareto designs has been proposed. The key idea is to find a minimum-distance modification of the design that leaves the operational bandwidth intact while correcting the power split error by solving an appropriately formulated constrained optimization sub-problem. The response gradients required by underlying linear expansion models are estimated using finite differentiation (FD). The correction procedure incurs a negligible computational overhead because perturbations for FD are already obtained during execution of the SDP algorithm.

As demonstrated using two examples of miniaturized rat-race couplers, a set of Pareto-optimal designs can be obtained at a cost corresponding to a few dozens of high-fidelity model simulations and with good control of the power split ratio even though only two primary objectives (size minimization and bandwidth maximization) are handled directly. Comparison of the refined corrected and uncorrected designs indicates that the correction scheme has an important effect on the power split error and maintaining the desired structure bandwidth. The numerical results are validated by measurements of the fabricated coupler prototypes.

Possible directions for the future research include application of extending the correction mechanism to control other performance characteristics of microwave structures such as phase shift, or bandwidth determined in terms of frequency range for which the power split error is

below a specified threshold. The technique could be also used for two-objective optimization of other structures with multiple performance characteristics, such as power dividers, multiplexers, or Butler matrices.

It should be noted that the proposed correction scheme constitutes a significant enhancement of the SDP framework that extends its applicability to problems that require handling more than two design requirements at a time. From this perspective, a direction for the future work is implementation of constraint handling capability directly into the SDP algorithm.

Acknowledgement

References

[1] Kurgan, P., Filipcewicz, J., Kitlinski, M. (2012). Development of a compact microstrip resonant cell aimed at efficient microwave component size reduction. *IET Microwaves, Ant. Prop*., 6(12), 1291–1298.

[2] Tseng, C.H., Chang, C.L. (2012). A rigorous design methodology for compact planar branch-line and rat-race couplers with asymmetrical T-structures. *IEEE Trans. Microwave Theory Tech*., 60(7), 2085–2092.

[3] Salari, M.A., Manoochehri, O., Abbasiniazare, S. (2013). Miniaturized microstrip ring hybrid with defected microstrip structure. *Microw. Opt. Tech. Lett*., 55(10), 2245–2248.

[4] Guo, L., Wang, S., Chen, X., Parini, C.G. (2010). Study of compact antenna for UWB applications. *Electronics Lett*., 46(2), 115–116.

[5] Gautam, A.K., Yadav, S., Kanaujia, B.K. (2013). A CPW-fed compact UWB microstrip antenna. *IEEE Ant. Wireless Prop. Lett*., 12, 151–154.

[6] Xiao, S., Wang, B.Z., Shao, W., Zhang, Y. (2005). Bandwidth-enhancing ultralow-profile compact patch antenna. *IEEE Trans. Ant. Prop*., 53(11), 3443–3447.

[7] Ahn, H.R., Bumman, K. (2008). Toward integrated circuit size reduction. *IEEE Microw. Mag*., 9(1), 65–75.

[8] Sani, A., Alomainy, A., Palikaras, G., Nechayev, Y., Yang. H., Parini, C., Hall, P.S. (2010). Experimental characterization of UWB on-body radio channel in indoor environment considering different antennas. *IEEE Trans. Ant. Prop*., 58(1), 238–241.

[9] Ning, H. (2013). *Unit and ubiquitous internet of things*. CRC Press.

[10] Al-Fuqaha, A., Guizani, M., Mohammadi, M., Aledhari, M., Ayyash, M. (2015). Internet of things: a survey on enabling technologies, protocols, and applications. *IEEE Communications Surveys & Tutorials*, 17(4), 2347–2376.

[11] Koziel, S., Bekasiewicz, A., Kurgan, P. (2015). Rapid multi-objective simulation-driven design of compact microwave circuits. *IEEE Microwave Wireless Comp. Letters*, 25(5), 277–279.

[12] Koziel, S., Bekasiewicz, A., Kurgan, P., Bandler, J.W. (2015). Rapid multi-objective design optimization of compact microwave couplers by means of physics-based surrogates. *IET Microwaves, Ant. Prop*., 10(5), 479–486.

[13] Liao, S.S., Sun, P.T., Chin, N.C., Peng, J.T. (2005). A novel compact-size branch-line coupler. *IEEE Microw. Wireless Comp. Lett.*, 15(9), 588–590.

[14] Xu, H.X., Wang, G.M., Lu, K. (2011). Microstrip rat-race couplers. *IEEE Microw. Mag.*, 12(4), 117–129.

[15] Jung, C., Negra, R., Ghannouchi, F.M. (2008). A design methodology for miniaturized 3-dB branch-line hybrid couplers using distributed capacitors printed in the inner area. *IEEE Trans. Microw. Theory Techn.*, 56(12), 2950–2953.

[16] Kurgan, P., Kitlinski, M. (2011). Doubly miniaturized rat-race hybrid coupler. *Microwave Opt. Tech. Lett.*, 53(6), 1242–1244.

[17] Bandler, J.W., Cheng, Q.S., Dakroury, S.A., Mohamed, A.S., Bakr, H.M., Madsen, K., Søndergaard, J. (2004). Space mapping: the state of the art. *IEEE Trans. Microwave Theory Tech.*, 52(1), 337–361.

[18] Koziel, S., Ogurtsov, S. (2014). *Antenna design by simulation-driven optimization. Surrogate-based approach*. Springer.

[19] Koziel, S., Yang, X.S., Zhang, Q.J. (eds.), (2013). *Simulation-driven design optimization and modeling for microwave engineering*. Imperial College Press.

[20] El Sabbagh, M.A., Bakr, M.H., Bandler, J.W. (2006). Adjoint higher order sensitivities for fast full-wave optimization of microwave filters. *IEEE Trans. Microw Theory Tech.*, 54, 3339–3351.

[21] Bakr, M.H., Nikolova, N.K. (2004). An adjoint variable method for time-domain transmission-line modeling with fixed structured grids. *IEEE Trans. Microwave Theory Tech.*, 52(2), 554–559.

[22] Khalatpour, A., Amineh, R.K., Cheng, Q.S., Bakr, M.H., Nikolova, N.K., Bandler, J.W. (2011). Accelerating space mapping optimization with adjoint sensitivities. *IEEE Microwave Wireless Comp. Lett.*, 21(6), 280–282.

[23] Bekasiewicz, A., Koziel, S. (2015). Efficient multi-fidelity design optimization of microwave filters using adjoint sensitivity. *Int. J. RF Microwave CAE*, 25(2), 178–183.

[24] Yeung, S.H., Man, K.F. (2011). Multiobjective optimization. *IEEE Microw. Mag.*, 12(6), 120–133.

[25] Deb, K. (2001). *Multi-Objective Optimization Using Evolutionary Algorithms*. NY: Wiley.

[26] Kuwahara, Y. (2005). Multiobjective Optimization Design of Yagi–Uda Antenna. *IEEE Trans. Ant. Prop.*, 53(6), 1984–1992.

[27] Chamaani, S., Abrishamian, M.S., Mirtaheri, S.A. (2010). Time-domain design of UWB Vivaldi antenna array using multiobjective particle swarm optimization. *IEEE Ant. Wireless Prop. Lett.*, 9, 666–669.

[28] Jin, N., Rahmat-Samii, Y. (2007). Advances in particle swarm optimization for antenna designs: real-number, binary, single-objective and multiobjective implementations. *IEEE Trans. Ant. Prop.*, 55(3), 556–567.

[29] Goudos, S.K., Zaharis, Z.D., Kampitaki, D.G., *et.al.* (2009). Pareto optimal design of dual-band base station antenna arrays using multi-objective particle swarm optimization with fitness sharing. *IEEE Trans. on Magn.*, 45, 1522–1525.

[30] Koziel, S., Bekasiewicz, A., Kurgan, P. (2015). Rapid multi-objective simulation-driven design of compact microwave circuits. *IEEE Microwave Wireless Comp. Lett.*, 25(5), 277–279.

[31] Koziel, S., Bekasiewicz, A., Zieniutycz, W. (2014). Expedited EM-driven multi-objective antenna design in highly-dimensional parameter spaces. *IEEE Ant. Wireless Prop. Lett.*, 13, 631–634.

[32] Koziel, S., Bekasiewicz, A. (2015). Fast multiobjective optimization of narrow-band antennas using RSA models and design space reduction. *IEEE Ant. Wireless Prop. Lett.*, 14, 450–453.

[33] Koziel, S., Ogurtsov, S. (2013). Multi-objective design of antennas using variable-fidelity simulations and surrogate models. *IEEE Trans. Ant. Prop.*, 61(12), 5931–5939.

[34] Koziel, S., Bekasiewicz, A. (2016). Multi-objective antenna design by means of sequential domain patching. *IEEE Ant. Wireless Prop. Lett.*, 15, 1089–1092.

[35] Bekasiewicz, A., Koziel, S., Pankiewicz, B. (2015). Accelerated simulation-driven design optimisation of compact couplers by means of two-level space mapping. *IET Microwaves, Ant. Prop.*, 9(7), 618–626.

[36] CST Microwave Studio, ver. 2015, CST AG, Bad Nauheimer Str. 19, D-64289 Darmstadt, Germany, 2015.

[37] Tseng, C.H., Chen, H.J. (2008). Compact rat-race coupler using shunt-stub-based artificial transmission lines. *IEEE Microw. Wireless Comp. Lett.*, 18(11), 734–736.

[38] Kotinis, M. (2010). A particle swarm optimizer for constrained multi-objective engineering design problems. *Eng. Optimization*, 42(10), 907–926.

[39] Al-Baity, H., Meshoul, S., Kaban, A. (2012). Constrained multi-objective optimization using a quantum behaved particle swarm. Huang, T., Zeng, Z., Li, C., Leung, C.S. (eds.). *Int. Conf. Neural Information Processing*, 456–464.

[40] Feliot, P., Bect, J., Vazquez, E. (2017). A Bayesian approach to constrained single- and multi-objective optimization. *J. Global Opt.*, 67(1), 1–37.

[41] Martinez-Frutos, J., Herrero-Perez, D. (2016). Kriging-based infill sampling criterion for constraint handling in multi-objective optimization. *J. Global Opt.*, 64(1), 97–115.

[42] Hussein, R., Deb, K. (2016). A generative kriging surrogate model for constrained and unconstrained multi-objective optimization. *Proc. Genetic Evolutionary Comp. Conf.*, 573–580.

[43] Bekasiewicz, A., Koziel, S., Leifsson, L. (2016). Sequential domain patching for computationally feasible multi-objective optimization of expensive electromagnetic simulation models. *Procedia Comp. Sci.*, 80, 1093–1102.

[44] Koziel, S., Bekasiewicz, A. (2016). Multi-objective optimization microwave couplers using corrected domain patching. *European Microwave Conference*, 1–4, London.